

## Observation of Instability-Induced Current Redistribution in a Spherical-Torus Plasma

J. E. Menard,<sup>1</sup> R. E. Bell,<sup>1</sup> D. A. Gates,<sup>1</sup> S. M. Kaye,<sup>1</sup> B. P. LeBlanc,<sup>1</sup> F. M. Levinton,<sup>2</sup> S. S. Medley,<sup>1</sup> S. A. Sabbagh,<sup>3</sup>  
D. Stutman,<sup>4</sup> K. Tritz,<sup>4</sup> and H. Yuh<sup>2</sup>

<sup>1</sup>*Princeton Plasma Physics Laboratory, Princeton, New Jersey, USA*

<sup>2</sup>*Nova Photonics Inc., Princeton, New Jersey, USA*

<sup>3</sup>*Columbia University, New York, New York, USA*

<sup>4</sup>*Johns Hopkins University, Baltimore, Maryland, USA*

(Received 16 April 2006; published 30 August 2006)

A motional Stark effect diagnostic has been utilized to reconstruct the parallel current density profile in a spherical-torus plasma for the first time. The measured current profile compares favorably with neoclassical theory when no large-scale magnetohydrodynamic instabilities are present in the plasma. However, a current profile anomaly is observed during saturated interchange-type instability activity. This apparent anomaly can be explained by redistribution of neutral beam injection current drive and represents the first observation of interchange-type instabilities causing such redistribution. The associated current profile modifications contribute to sustaining the central safety factor above unity for over five resistive diffusion times, and similar processes may contribute to improved operational scenarios proposed for ITER.

DOI: [10.1103/PhysRevLett.97.095002](https://doi.org/10.1103/PhysRevLett.97.095002)

PACS numbers: 52.55.Fa, 52.55.Pi, 52.55.Tn, 52.55.Wq

The spherical-torus (ST) configuration [1], a more compact version of the standard tokamak, has made considerable progress in achieving the high energy confinement [2] and efficient utilization of the externally applied magnetic field [3–6] required for efficient fusion energy applications. Recent progress has also been achieved in integrating high energy confinement and magnetic field utilization to achieve a high fraction of plasma current not generated by the usual inductive transformer action of the tokamak [7,8]. A high noninductive current fraction is deemed essential for the ST concept due to the necessarily compact central column and transformer used for the inductive current drive. Advanced tokamaks have recently achieved high magnetic field utilization and high noninductive current fraction [9] utilizing a combination of self-generated “bootstrap” current [10], neutral beam injection current drive (NBICD), and electron cyclotron wave current drive. However, given the difficulty in achieving fully noninductive operation, alternative discharge scenarios have also been developed in which a majority of the current is driven by the bootstrap effect, but inductive current drive is still a significant fraction of the total current [11–13]. A necessary element of such scenarios is the avoidance of rapidly growing core magnetic reconnection events which can trigger slowly growing but potentially disruptive tearing instabilities. This avoidance can be achieved by maintaining the core safety factor at or above unity using auxiliary current drive and/or through the action of other comparatively benign magnetohydrodynamic (MHD) instabilities.

A key scientific advance in understanding current drive physics in the absence of MHD activity has been the validation of neoclassical resistivity, bootstrap current, and other sources of noninductive current coupled with measurements of the internal inductive electric field [14]. In this Letter, we report on the first systematic study of

neoclassical and beam-driven currents in a low aspect ratio tokamak plasma. These studies are made possible by a new motional Stark effect (MSE) diagnostic technique [15] developed specifically for the low toroidal magnetic field strength ( $B_T \leq 0.6$  T) of present-day ST devices. Similar to standard aspect ratio tokamaks, the national spherical-torus experiment (NSTX) [16] has now demonstrated discharge scenarios in which a majority of the current is driven noninductively and the minimum safety factor  $q_{\min}$  is maintained at or above unity for durations limited only by coil heating limits. In the longest duration plasmas obtained thus far in NSTX, sustained elevated central  $q$  can be achieved via operation at a high bootstrap current fraction or from the action of saturated MHD activity. In this Letter, we focus on the role of MHD activity in promoting elevated central  $q$ . In particular, saturated core-localized interchange-type modes (termed “SCI” modes in this Letter) are identified for the first time as a means of redistributing injected energetic particle current resulting in elevated central  $q$ . The remainder of this Letter describes the triggering, structure, and identification of these modes followed by evidence for and explanation of the observed current redistribution.

Equilibrium reconstructions constrained by MSE data underpin the studies of current profile evolution and mode stability and dynamics described in this Letter. The NSTX MSE system for the data analyzed here consists of 8 mid-plane channels covering the inner 90% of the plasma normalized minor radius  $\rho \equiv \hat{\psi}^{1/2}$ , where  $\psi \equiv RA_\phi$ ,  $A_\phi$  is the toroidal component of the equilibrium magnetic vector potential, and  $\hat{\psi} \equiv (\psi - \psi_{\text{axis}})/(\psi_{\text{edge}} - \psi_{\text{axis}})$ . The reconstructed current profiles are most accurate in the plasma core, since 7 of the 8 channels are typically inside  $\rho = 0.6$ . A 51 point midplane horizontally viewing carbon impurity charge exchange recombination spectroscopy system is

used to determine the electric field profile from impurity radial force balance to correct the MSE pitch angle data [17]. Toroidal-rotation-induced deviations of density and pressure from flux functions [18] are accounted for by using flux-surface averages in the evaluation of the neo-classical terms [19] and in MHD stability calculations.

In tokamaks and STs, normalized magnetic utilization efficiencies are commonly expressed in terms of a parameter  $\beta_N$ , where  $\beta$  is the ratio of the plasma kinetic pressure to magnetic field pressure and  $\beta_N$  removes the intrinsic scaling of  $\beta$  with plasma current, applied magnetic field, and plasma minor radius. Figure 1(a) shows the  $n = 1$  ( $n$  is the instability toroidal mode number and  $n = 1$  is typically the most unstable mode) stability threshold  $\beta_N \approx 3.8$ –4.2 computed using the DCON code [20] ignoring the influence of the resistive conducting wall of NSTX. Treating the resistive wall as ideal (superconducting), the computed  $n = 1$  stability limit is  $\beta_N \approx 5.5$ –5.7 near  $t = 0.9$  s. The experimental  $\beta_N$  value exceeds the computed no-wall limit from  $t = 0.4$  to 1.05 s and is very close to the ideal-wall limit near  $t = 0.9$  s consistent with plasma rotation and mode dissipation stabilizing the resistive wall mode allowing sustained operation near the ideal-wall limit [21,22]. Several rapid but temporary decreases in  $\beta_N$  (correlated with  $n = 1$  instability bursts) are observable in Fig. 1(a) when  $\beta_N$  is near the computed ideal-wall limit. However, the experimental  $\beta_N$  never recovers from the final  $\beta_N$  collapse near  $t = 1.05$  s. As seen in Fig. 1(b), this time coincides with the onset of a continuous  $n = 1$  mode with frequency  $f = 5$ –8 kHz. Since the neutral beam heating power is held fixed at 6 MW for  $t \geq 0.16$  s, reduced  $\beta_N$  after  $t = 1.05$  s apparently results from the SCI mode degrading confinement. These results indicate that the

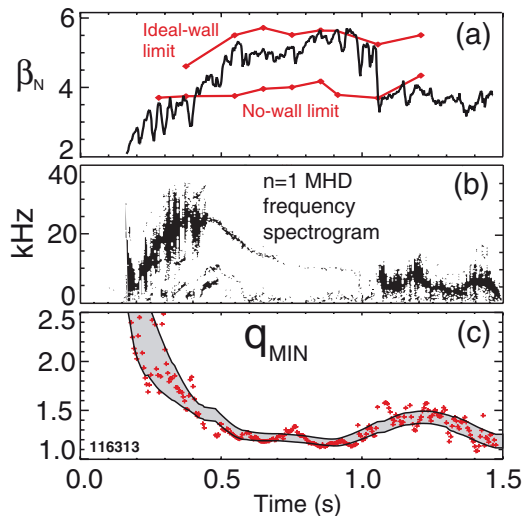


FIG. 1 (color). (a) Normalized beta (black line), calculated  $n = 1$  no-wall and ideal-wall stability limits (red line), (b)  $n = 1$  MHD activity frequency spectrogram, and (c) reconstructed instantaneous (red) and 200 ms time-average (gray) minimum  $q$  value.

SCI mode is apparently triggered by repeated excursions above the  $n = 1$  ideal-wall limit and, once triggered, can persist for the remainder of the discharge. Figure 1(c) shows that the onset of the SCI mode also has a significant impact on the safety factor evolution. Prior to mode onset during the high  $\beta_N$  phase, the minimum safety factor value is nearly constant with  $q_0 = q_{\min} = 1.15$ –1.25. Just after mode onset, the  $q_{\min}$  value abruptly increases to 1.3–1.4 and remains above the pre-onset value until  $t = 1.4$  s when the toroidal magnetic field is ramped down due to coil heating limits. The estimated current redistribution time during the high- $\beta_N$  phase is 0.25–0.3 s [23], and the energy confinement time  $\tau_E = 35$  ms, so  $q_{\min}$  remains above unity for many current redistribution times and several tens of energy confinement times.

The structure of the SCI mode can be determined from inversion [18] of ultrasoft x-ray (USXR) line-integrated emission data [24]. Figure 2(a) shows the line-integrated emission data in the plasma core during mode activity, and Fig. 2(b) shows the best fit to the total emission obtained assuming a plasma displacement  $\vec{\xi}$  with helicity  $m/n = 1/1$ . The USXR data cannot be well-fit using a 2/1 island eigenfunction [18] as would be expected for a 2/1 neo-classical tearing mode (NTM). Figure 2(c) shows the time evolution of the best-fit flux-surface-normal displacement profile  $\vec{\xi}(\rho) \cdot \nabla\rho/|\nabla\rho|$  at the outboard midplane. As seen in the figure, the maximum displacement is approximately 1.6 cm at  $\rho = 0.4$ . The eigenfunction is evidently initially quite broad with finite amplitude extending to  $\rho \approx 0.8$ ,

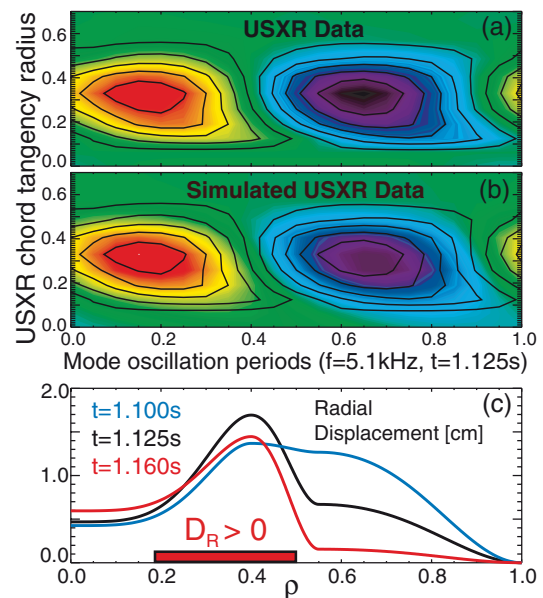


FIG. 2 (color). (a) Measured line-integrated USXR emission amplitude contours plotted versus chord tangency  $\rho$  and time for one oscillation period, (b) best-fit simulated USXR emission amplitude assuming a 1/1 helicity eigenfunction, and (c) reconstructed radial displacement amplitude profile at outboard midplane during mode saturation. The black contour lines in (a) and (b) are from the data in (a).

while at later times the eigenfunction narrows to have almost zero displacement outside  $\rho = 0.5$ . After  $t = 1.14$  s, the eigenfunction shape is measured to change little, and the poloidal magnetic field fluctuation amplitude measured at the outboard vacuum vessel wall remains approximately constant at 3–5 Gauss rms. Both trends are consistent with mode saturation. During the saturated phase, the reconstructed  $q$  profile is flat to weakly reversed with  $q_0 - q_{\min} \approx 0.1$  and  $\rho_{q_{\min}} = 0.3$ – $0.45$ . As shown in Fig. 2(c), such profiles are calculated to be resistive interchange unstable ( $D_R > 0$ ) [25] at  $t = 1.16$  s for  $\rho = 0.2$ – $0.5$ . Scans of the plasma  $\beta$  and current find resistive interchange instability requires  $\beta_N > 3.6$  and  $q_{\min} < 1.3$ , and internal  $n = 1$  ideal modes become unstable for  $q_{\min} < 1.1$  and  $\beta_N > 3.9$ . Thus, the observed mode may be a saturated nonresonant version of the resistive interchange mode [26] or a quasi-interchange mode [27].

Inference of current redistribution from the SCI mode relies heavily on calculation of the total current density profile. For the calculations described here, the neoclassical conductivity  $\sigma_{nc}$  and bootstrap current are calculated from theory valid for general geometry and low aspect ratio [28], and the beam current drive is calculated using the TRANSP code [29]. The inductive current density is calculated from  $\langle \vec{J}_{IND} \cdot \vec{B} \rangle \equiv \sigma_{nc} \langle \vec{E} \cdot \vec{B} \rangle$ , where the inductive electric field  $\vec{E} = -\partial \vec{A} / \partial t$ ,  $\vec{A}$  is the total (poloidal plus toroidal) vector potential obtained from the equilibrium reconstructions [14], and  $\langle \rangle$  is the flux-surface averaging operator. Avoiding time intervals of rapidly varying plasma parameters and using a 200 ms smoothing interval for  $\langle \vec{E} \cdot \vec{B} \rangle$ , Fig. 3(a) shows that the total calculated current agrees with the measured total to within 5%. Figure 3(a) also illustrates that NSTX discharges can sustain a majority of the plasma current noninductively with up to 60% of the current driven by the neoclassical bootstrap effect, neutral beam injection current drive, and toroidal components of the Pfirsch-Schlüter and diamagnetic currents. As seen in Fig. 3(b), the calculated total current density profile is also in good agreement with the reconstructed profile during the MHD-quiescent phase at high  $\beta_N$ . In contrast, after the onset of the SCI mode, the density slowly decreases and the electron pressure profile peaking increases. These changes cause the calculated bootstrap and beam-driven currents to increase in the plasma core, and, as shown in Fig. 3(c), the calculated central current density exceeds the reconstructed value by 45%. Understanding how the experimentally broadened current profile is maintained after  $t = 1.05$  s is a key result of this Letter.

Tearing modes [30,31] and Alfvén instabilities [32] have previously been identified as capable of causing energetic particle diffusion and loss via orbit stochasticization, and the interchange-type instability described above could enhance fast-ion diffusion via similar mechanisms. For comparison, the SCI flux-surface-normal magnetic field perturbation amplitude inside  $\rho = 0.45$  estimated from the USXR data [18] is as much as an order of magnitude

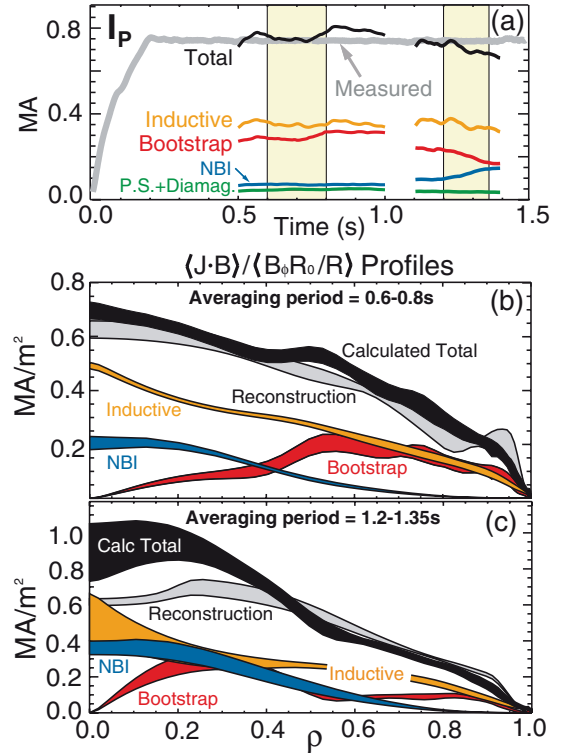


FIG. 3 (color). (a) Measured (gray line) and calculated (black line) total plasma currents with inductive and noninductive contributions also plotted, (b) comparison of the time-averaged reconstructed (gray) and calculated (black) parallel current density profile for  $t = 0.6$ – $0.8$  s, and (c) for  $t = 1.2$ – $1.35$  s. (a)–(c) assume no anomalous fast-ion diffusion, and the profile uncertainties in (b) and (c) are mean absolute errors of the time averages.

higher than reported previously [31], so very large fast-ion diffusivities may be possible. For the results described here, the total neutron rate is the only available direct measurement of changes in the fast-ion population. During the discharge phase when no SCI mode activity is present, the total neutron rate calculated by TRANSP is approximately 10% higher than the measured value which is within the experimental uncertainty of the measurement. Figure 4(a) plots calculated neutron rates multiplied by 0.9 to match the measured value during the time interval  $t = 0.9$ – $0.95$  s. From this renormalization, an additional 20%–30% decrease in neutron rate relative to calculation is evident after SCI mode onset, assuming no anomalous fast-ion diffusion. From this decrease, it is inferred that the SCI mode is modifying the fast-ion population and possibly the NBICD.

Fast-ion diffusion can be modeled in TRANSP using a time and spatially dependent diffusivity for the slowing-down ions from NBI. For the time period from  $t = 1.05$ – $1.15$  s, Fig. 2(c) shows that the eigenfunction radial extent is broader than during the mode saturation phase, and a constant anomalous fast-ion diffusivity  $\chi_{fast} = 15 \text{ m}^2 \text{ s}^{-1}$  extending from  $\rho = 0.0$ – $0.7$  can reproduce the measured neutron rate during this time interval. After

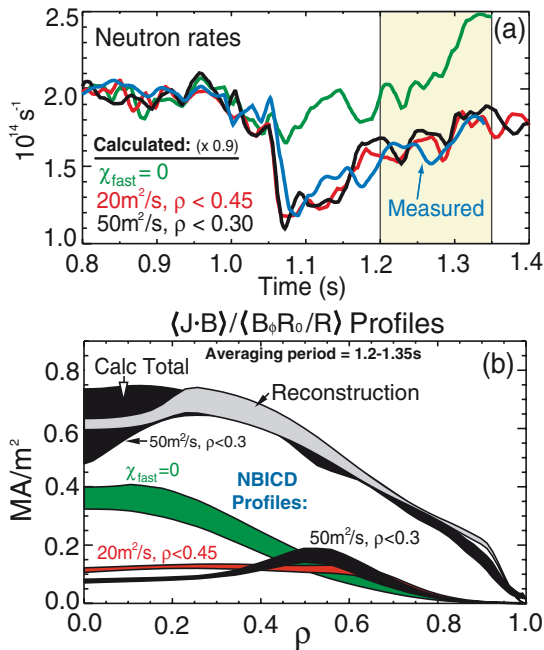


FIG. 4 (color). (a) Measured (blue line) and calculated neutron rates ( $\times 0.9$ ) and (b) comparison of reconstructed (gray) and calculated (black) total parallel current density profile for  $t = 1.2$ – $1.35$  s for the best-fit fast-ion diffusivity model. NBICD profiles for the diffusivities of (a) are also shown.

$t = 1.15$  s, the best simultaneous match to the subsequent neutron rate evolution and reconstructed current density profile is obtained with  $\chi_{\text{fast}} = 50 \text{ m}^2 \text{ s}^{-1}$  inside  $\rho = 0.3$ . As seen in Fig. 4(a), this nonzero fast-ion diffusivity assumption reproduces the measured neutron rate evolution after SCI onset. Perhaps more consistent with the mode extent from the USXR data,  $\chi_{\text{fast}} = 20 \text{ m}^2 \text{ s}^{-1}$  inside  $\rho = 0.45$  also reproduces the measured neutron rate. As shown in Fig. 4(b), this simulated redistribution of fast ions reduces the calculated total current density in the core from 45% higher than the reconstructed value to the same value to within the uncertainty of the calculation. Further, the NBICD density is increased by 20%–40% for  $\rho = 0.5$ – $0.6$ , resulting in a flat to hollow NBICD profile. The total NBICD and fast-ion stored energy are reduced by only 15% for the two diffusion models shown, so most of the NBICD is apparently redistributed rather than lost.

In summary, the NSTX results described above imply that core MHD activity can induce fast-ion redistribution and convert a centrally peaked NBICD profile into a flat or even hollow profile. This conversion apparently raises the safety factor in the plasma core, producing a flat to weakly reversed-shear  $q$  profile which destabilizes core-localized  $n = 1$  interchange-type instabilities which saturate and help sustain a broadened NBICD profile and elevated safety factor. It is noteworthy that, for the  $q$  profile characteristics described above, interchange modes are potentially self-regulating since they become more unstable as  $q_{\text{min}}$  is lowered, thereby increasing fast-ion diffusion and raising  $q_{\text{min}}$ . Self-regulation may also occur through the

plasma pressure, since these modes degrade plasma energy confinement and  $\beta$ , which decreases the instability drive. Similar mode dynamics and MHD-induced NBICD diffusion may also be relevant to tokamak scenarios proposed for ITER [33] in which 3/2 NTMs have previously been reported to aid sustainment of the central  $q$  above unity for extended durations [34].

This research was supported by the United States Department of Energy under Contract No. DE-AC02-76CH03037 (PPPL) and Grants No. DE-FG02-99ER54524 (CU) and No. DE-FG02-99ER54523 (JHU).

- [1] Y.-K.M. Peng and D.J. Strickler, Nucl. Fusion **26**, 769 (1986).
- [2] R. Maingi *et al.*, Phys. Rev. Lett. **88**, 035003 (2002).
- [3] M. Gryaznevich *et al.*, Phys. Rev. Lett. **80**, 3972 (1998).
- [4] S.A. Sabbagh *et al.*, Phys. Plasmas **9**, 2085 (2002).
- [5] J.E. Menard *et al.*, Nucl. Fusion **43**, 330 (2003).
- [6] D. Gates and the NSTX National Research Team, Phys. Plasmas **10**, 1659 (2003).
- [7] J.E. Menard *et al.*, Phys. Plasmas **11**, 639 (2004).
- [8] D. Gates *et al.*, Nucl. Fusion **46**, S22 (2006).
- [9] M. Murakami *et al.*, Phys. Rev. Lett. **90**, 255001 (2003).
- [10] R.J. Bickerton, J.W. Connor, and J.B. Taylor, Nature (London), Phys. Sci. **229**, 110 (1971).
- [11] M.R. Wade *et al.*, Phys. Plasmas **8**, 2208 (2001).
- [12] A.C.C. Sips *et al.*, Plasma Phys. Controlled Fusion **44**, B69 (2002).
- [13] E. Joffrin *et al.*, Nucl. Fusion **45**, 626 (2005).
- [14] C.B. Forest *et al.*, Phys. Rev. Lett. **73**, 2444 (1994).
- [15] F. Levinton, Bull. Am. Phys. Soc. **49**, 221 (2004).
- [16] S. Kaye *et al.*, Nucl. Fusion **45**, S168 (2005).
- [17] B.W. Rice, K.H. Burrell, and L.L. Lao, Nucl. Fusion **37**, 517 (1997).
- [18] J.E. Menard *et al.*, Nucl. Fusion **45**, 539 (2005).
- [19] F.L. Hinton and S.K. Wong, Phys. Fluids B **28**, 3082 (1985).
- [20] A. Glasser and M. Chance, Bull. Am. Phys. Soc. **42**, 1848 (1997).
- [21] A.M. Garofalo *et al.*, Phys. Rev. Lett. **89**, 235001 (2002).
- [22] A.C. Sontag *et al.*, Phys. Plasmas **12**, 056112 (2005).
- [23] D.R. Mikkelsen, Phys. Fluids B **1**, 333 (1989).
- [24] D. Stutman *et al.*, Rev. Sci. Instrum. **70**, 572 (1999).
- [25] A. Glasser, J. Greene, and J. Johnson, Phys. Fluids **18**, 875 (1975).
- [26] M.S. Chu *et al.*, Phys. Rev. Lett. **77**, 2710 (1996).
- [27] C. Wahlberg, Plasma Phys. Controlled Fusion **47**, 757 (2005).
- [28] O. Sauter, C. Angioni, and Y.R. Lin-Liu, Phys. Plasmas **6**, 2834 (1999).
- [29] R.J. Goldston, D.C. McCune, and H.H. Towner, J. Comput. Phys. **43**, 61 (1981).
- [30] C.B. Forest *et al.*, Phys. Rev. Lett. **79**, 427 (1997).
- [31] E.M. Carolipio, W.W. Heidbrink, C.B. Forest, and R.B. White, Nucl. Fusion **42**, 853 (2002).
- [32] K.L. Wong *et al.*, Phys. Rev. Lett. **93**, 085002 (2004).
- [33] ITER Physics Basis, Nucl. Fusion **39**, 2137 (1999).
- [34] T.C. Luce and the DIII-D Team, Nucl. Fusion **45**, S86 (2005).